

This work was written as part of one of the author's official duties as an Employee of the United States Government and is therefore a work of the United States Government. In accordance with 17 U.S.C. 105, no copyright protection is available for such works under U.S. Law. Access to this work was provided by the University of Maryland, Baltimore County (UMBC) ScholarWorks@UMBC digital repository on the Maryland Shared Open Access (MD-SOAR) platform.

Please provide feedback

Please support the ScholarWorks@UMBC repository by emailing scholarworks-group@umbc.edu and telling us what having access to this work means to you and why it's important to you. Thank you.

Experimental study of Bloch vector analysis in nonlinear, finite, dissipative systemsG. D'Aguanno,^{1,2,*} M. C. Larciprete,³ N. Mattiucci,^{1,2} A. Belardini,³ M. J. Bloemer,² E. Fazio,³
O. Buganov,⁴ M. Centini,³ and C. Sibilia³¹*Aegis Technologies, Microsystems/Nanotechnology, 410 Jan Davis Drive, Huntsville, Alabama 35806, USA*²*C. M. Bowden Facility, Building 7804, RDECOM, Redstone Arsenal, Alabama 35898, USA*³*CNISM and Dipartimento di Energetica, Sapienza Università di Roma Via A. Scarpa 16, I-00161 Roma, Italy*⁴*Institute of Molecular and Atomic Physics, NASB, Minsk BY-220072, Belarus*

(Received 26 June 2009; published 28 January 2010)

We have investigated and experimentally demonstrated the applicability of the Bloch vector for one-dimensional, nonlinear, finite, dissipative systems. The case studied is the second harmonic generation from metallodielectric multilayer filters. In particular, we have applied the Bloch vector analysis to Ag/Ta₂O₅ thin-film multilayer samples and shown the importance of the phase matching calculated through the Bloch vector. The nonlinear coefficients extracted from experimental results are consistent with previous studies. Nowadays, metal-based nanostructures play a fundamental role in nonlinear nanophotonics and nanoplasmonics. Our results clearly suggest that even in these forefront fields the Bloch vector continues to play an essential role.

DOI: [10.1103/PhysRevA.81.013834](https://doi.org/10.1103/PhysRevA.81.013834)

PACS number(s): 42.70.Qs, 42.25.Bs, 42.65.Ky

I. INTRODUCTION

The Bloch theorem and the Bloch vector are central in many fields of physics, ranging from solid-state physics [1] to optics and photonics [2]. Anywhere the periodic repetition of elements in one, two, or three dimensions (1D, 2D, 3D)—be they atoms, molecules, thin layers of materials, or any generic building block—gives rise to allowed and forbidden bands for wave propagation, the Bloch vector plays a leading role in describing the band structure [1,2]. In this article we focus on simple 1D periodic systems (layered structures or Bragg gratings [2]) because of their intrinsically simpler fabrication procedures and easier theoretical analysis than multidimensional systems, although they retain many of the characteristics of more complicated structures. A Bragg grating or 1D photonic crystal (PC) in its simplest realization is basically made of a periodic repetition of two layers of materials with different refractive indices which form the elementary cell (or building block) of the structure. This periodic repetition gives rise to allowed and forbidden bands for light propagation [2] in analogy with the allowed and forbidden bands for electronic propagation in semiconductors [1]. We can distinguish purely dielectric Bragg gratings and metallodielectric (MD) structures, both can be fabricated by standard sputtering or thermal evaporation techniques [3]. The Bloch vector for a 1D periodic structure comes directly from the Bloch theorem and can be written as [4]

$$K_{\beta}(k_x, \omega) = \frac{1}{\Lambda} \cos^{-1} \left[\frac{1}{2}(m_{11} + m_{22}) \right], \quad (1)$$

where \cos^{-1} is the inverse cosine (arccosine) function; k_x is the transverse wave vector along the x axis, that is, in the direction perpendicular to the periodicity (z axis); Λ is the length of the elementary cell of the structure; and $\hat{M} = (m_{1,1}, m_{1,2}; m_{2,1}, m_{2,2})$ is the transfer matrix (or scattering matrix) of the elementary cell. Equation (1) comes from the Bloch theorem, which is applicable for a *strictly* periodic

potential. One may ask what happens when the structure under investigation is made of so few periods that it is intrinsically finite and periodic boundary conditions cannot be applied (finite structure). Moreover, what happens when the materials involved are dissipative and nonlinear? These deceptively simple questions have been the subject of intense theoretical investigation over the last two decades [5–12]. One simple way to approach the problem is to note that a Bloch vector defined as in Eq. (1) can be always calculated, regardless of the strict applicability of the Bloch theorem, because it depends on the trace of the scattering matrix of the elementary cell. In other words, Eq. (1) can be calculated no matter the number of the elementary cells that actually compose the structure and whether the structure is dissipative or has a nonlinear response. Of course, the question that arises is whether this “generalized Bloch vector” continues to give useful information, especially when, as in our case, one deals with nonlinear, dissipative structures of only few periods in length. In order to shed some light on the question, we study the second harmonic generation (SHG) processes from three MD structures and examine the possibility of interpreting the results in the framework of a Bloch vector analysis. The article is organized as follows: In Sec. II we describe the samples preparation and the experimental setup. In Sec. III we outline the theoretical model used for SHG and compare the experimental and theoretical results. In Sec. IV we interpret the results in the framework of a Bloch vector analysis and in Sec. V we give our conclusions.

II. SAMPLES PREPARATION AND EXPERIMENTAL SETUP

The three samples [sample (a), sample (b), and sample (c)] are made of $N = 5$ periods of alternating layers of Ag and Ta₂O₅. The elementary cells of the samples are: (a) Ag (~ 21 nm)/Ta₂O₅ (~ 122 nm), (b) Ag (~ 18 nm)/Ta₂O₅ (~ 152 nm), (c) Ag (~ 18 nm)/Ta₂O₅ (~ 169 nm). Note that in all three samples the amount of Ag is roughly the same. All depositions were carried out by magnetron sputtering onto 1-mm-thick, optically flat ($\lambda/20$) glass substrates. After

*Corresponding author: giuseppe.daguanno@us.army.mil

deposition was completed, a linear optical characterization of the samples was carried out. The transmittance spectra were recorded at normal incidence in the visible-NIR range by spectrophotometer and the experimental curves were modeled with a standard transfer-matrix method [4]. The optical constants for Ag used to fit the data were taken from the book of Palik [13], and the optical constants for Ta₂O₅ were taken from previously measured data [14] of the reflectance of a single Ta₂O₅ film deposited on Si with a Filmetrics reflectometer having a lower wavelength range of 600 nm and extrapolated to shorter wavelengths. Details of the sample fabrication are provided in Ref. [14]. The measured linear transmission spectra are in good agreement with the theoretical fits [14]. In particular, we take the relative permittivity of the materials as follows: $\epsilon_{\text{Ag}}(800 \text{ nm}) = -27.95 + 1.52i$, $\epsilon_{\text{Ag}}(400 \text{ nm}) = -3.77 + 0.67i$, $\epsilon_{\text{Ta}_2\text{O}_5}(800 \text{ nm}) = 4.6 + 0.027i$ and $\epsilon_{\text{Ta}_2\text{O}_5}(400 \text{ nm}) = 4.84 + 0.088i$.

The optical constants for Ta₂O₅ are consistent with published data [15]. Note that all the materials have an imaginary part of the permittivity and therefore have some degree of dissipation both at the fundamental frequency (FF) and the second harmonic (SH) frequency. In our samples the only source of quadratic nonlinearity is assumed to be in the metal layers. We measured the reflected SH signal at 400 nm for different polarization states of the fundamental input beam, intensities, and incident angles. The fundamental beam was provided by the output of a femtosecond Ti:sapphire laser ($\lambda = 800 \text{ nm}$, 1 kHz repetition rate, 150 fs pulse width), focused close to the sample with a lens of 150 mm focal length. The sample was placed on a rotational stage which allowed setting of the incidence angle with a resolution of 0.5°. The transverse profile of the fundamental beam was measured to be Gaussian with a spot size w of $\sim 600 \mu\text{m}$, corresponding to a peak power of $\sim 6 \text{ GW/cm}^2$. Fundamental and generated beam polarization states can be selected by rotating a half-wave plate and a linear analyzer, respectively. A long pass filter was used after the half-wave plate in order to avoid the spurious SH signal produced by the plate's crystals themselves due to the short pulse duration. After being reflected by the sample, the fundamental beam was suppressed, thus ensuring that only the SH beam was directed to the photomultiplier tube, and then analyzed with a 500-MHz digital oscilloscope. The calibration curve of the photomultiplier response was accurately performed with a reference β barium borate crystal. Experimental measurements performed under different polarization states of the FF show that the largest signal is recorded when the polarization of fundamental beam is set to \hat{p} (transverse magnetic), while the SH signal is \hat{p} polarized for both \hat{s} (transverse electric) and \hat{p} fundamental beam polarization, as expected [16]. This first set of measurements on all the samples was done by increasing the FF peak power and verifying the quadratic dependence of the SH signal on the FF peak power.

III. THEORETICAL MODEL AND EXPERIMENTAL RESULTS

The theoretical model to explain the SHG in the MD structure follows the classical approach outlined by Shen [17]. The quadratic nonlinearity of metals is described through two terms: the Lorentz term and the surface term. The Lorentz

term is

$$(\text{Lorentz term}) = 2i\omega\gamma(z)(\vec{E}_\omega \times \vec{H}_\omega), \quad (2)$$

where $\gamma(z) = \gamma$ in the metal layers and $\gamma(z) = 0$ in the dielectric layers. As is obvious from its name, it accounts for the Lorentz force exerted on the free electrons of the metal. The surface term is

$$(\text{surface term}) = d_S^{(2)} \sum_k \delta(z - z_k) : \vec{E} \vec{E}, \quad (3)$$

where $\delta(z - z_k)$ is the Dirac delta function calculated at the k th metal-dielectric interface just inside the metal, and the symbol “:” denotes the tensor product [17]. The surface term accounts for the second-order susceptibility at each metal-dielectric interface due to symmetry breaking. For TM polarization, in a Cartesian, right-handed, reference system (x, y, z) where z is the direction of the stratification of the structure, considering only the (z, z, z) component of the nonlinearities (i.e., $\text{TM} \rightarrow \text{TM SH}$ emission), the Helmholtz equation in meter-kilogram-second ampere units for the SH H field polarized along the y axis can be written as

$$\begin{aligned} \frac{d^2 H_{y,2\omega}}{dz^2} + \left\{ \left[\frac{2\omega}{c} n_{2\omega}(z) \right]^2 - [2k_{x,\omega}^{(\text{in})}]^2 \right\} H_{y,2\omega} \\ = 4\omega k_{x,\omega}^{(\text{in})} \left[\epsilon_0 d_S^{(2)} \sum_k \delta(z - z_k) E_{z,\omega}^2 + \frac{2i\omega}{c^2} \gamma(z) E_{x,\omega} H_{y,\omega} \right], \end{aligned} \quad (4)$$

where $k_{x,\omega}^{(\text{in})} = (n_{\text{in},\omega}\omega/c) \sin(\vartheta)$ is the transverse momentum of the incident FF pump field, ϑ is the incident angle of the pump field on the sample, $n_{\text{in},\omega}$ is the refractive index of the incident medium (air in our case) at the FF, $n_{2\omega}(z)$ is the step-varying, complex refractive index at the SH along the direction of the stratification, $\epsilon_0 \cong 8.85 \times 10^{-12} \text{ F/m}$ is the vacuum permittivity, and c is the speed of light *in vacuo*. $E_{x,\omega}$ is the x component of the FF electric field while $H_{y,\omega}$ is the FF magnetic field. In our model, the two “free parameters” are γ and the surface nonlinearity $d_S^{(2)}$, which will be compared with previously published data on SHG from single Ag films [18]. From Eq. (4) we note that we are looking for the SH emission that conserves the transverse momentum; in other words, the transverse momentum of the generated SH field is supposed to be at twice the transverse momentum of the incident pump field: $k_{x,2\omega} = 2k_{x,\omega}^{(\text{in})}$. We suppose that the FF field remains undepleted, allowing its calculation through a standard, linear matrix transfer technique [4]. At each interface the boundary conditions appropriate for TM polarization are considered [4]. Note that in the Lorentz term at the right-hand side of Eq. (4) we have included only the component oriented along the z direction as it is the dominant term according to experiments [18]. In the undepleted regime, Eq. (4) can be solved using a Green function approach for multilayered structures developed in Ref. [19,20] and adapted in this case to handle TM polarization. In particular, the SH magnetic field inside the multilayer located between $z = 0$ and $z = L$ can be

expressed as

$$H_{y,2\omega}(z) = 4\omega k_{x,\omega}^{(\text{in})} \int_0^L \frac{G_{2\omega}^{(\text{TM})}(z, \xi)}{\varepsilon_{2\omega}(\xi)} \left[\varepsilon_0 d_s^{(2)} \sum_k \delta(\xi - z_k) E_{z,\omega}^2(\xi) + \frac{2i\omega}{c^2} \gamma(\xi) E_{x,\omega}(\xi) H_{y,\omega}(\xi) \right] d\xi, \quad (5)$$

where $\varepsilon_{2\omega}(\xi)$ is the relative permittivity profile at the SH, and $G_{2\omega}^{(\text{TM})}(z, \xi)$ is the Green function for the multilayer calculated according to theory developed in Refs. [19,20], generalized here for TM polarization:

$$G_{2\omega}^{(\text{TM})}(z, \xi) = \frac{\varepsilon_{\text{out},2\omega}}{2ik_{z,2\omega}^{\text{out}} t_{2\omega}^{\text{out}}} \times \begin{cases} \Phi_{2\omega}^{(+)}(\xi) \Phi_{2\omega}^{(-)}(z), & 0 \leq z \leq \xi \\ \Phi_{2\omega}^{(+)}(z) \Phi_{2\omega}^{(-)}(\xi), & \xi \leq z \leq L \end{cases} \quad (6)$$

In Eq. (6), $\varepsilon_{\text{out},2\omega}$ is the relative permittivity at the SH of the output medium, the glass substrate in our case; $t_{2\omega}^{\text{out}}$ is the complex, linear, transmission function of the multilayer at the SH calculated in the output medium; $k_{z,2\omega}^{\text{out}} = \sqrt{(k_{0,2\omega} n_{\text{out},2\omega})^2 - (2k_{x,\omega}^{(\text{in})})^2}$ is the longitudinal momentum at the SH calculated in the output medium, $k_{0,2\omega} = 2\omega/c$ is the vacuum wave vector at the SH; and $\Phi_{2\omega}^{(+/-)}(z)$ are, respectively, the left-to-right (LTR)/right-to-left (RTL) linear modes of the structure at the SH calculated by a standard matrix transfer technique supposing a magnetic field of unitary amplitude incident onto the structure from LTR/RTL, respectively, with a transverse momentum $2k_{x,\omega}^{(\text{in})}$ in both cases [19,20].

The experimental data of the conversion efficiency of the reflected SHG versus incident angle ϑ for the three samples are reported in Fig. 1, which also shows the comparison with the theoretical predictions. The polarization direction of both fundamental and SH-generated electric fields lay in the plane of incidence (TM \rightarrow TM). For all the investigated multilayer structures, the SH signal displays a maximum value at an incidence angle of $\sim 55^\circ$, instead of $\sim 70^\circ$, which

is expected for the single Ag layer [16]. The figure also has a table of the fitted values of the nonlinearity for the three samples. We note that sample (a) and sample (b) have approximately the same values of nonlinearity, although the maximum conversion efficiency of sample (a) is one order of magnitude greater than the maximum conversion efficiency of sample (b). We also note that sample (c) appears to have much smaller values of the nonlinearities with respect to the first two samples.

SHG efficiency from single Ag films is highly dependent on the surface properties of the Ag [18]. Samples (a), (b), and (c) have multiple Ag films which could exacerbate any surface anomaly in the individual samples. We point out that in our approach the parameters γ and $d_s^{(2)}$ must be intended as ‘‘phenomenological parameters’’ in some way similar to those introduced in Ref. [21]. Nevertheless, by considering an effective component of the (z, z, z) nonlinearity $d_{\perp}^{(2)} \approx (1/2)[\gamma + d_s^{(2)}]$ as the dominant nonlinearity for TM \rightarrow TM emission, in agreement with the experimental results of Ref. [18], we find that the three samples have, respectively, the following values of effective nonlinearity: $d_{\perp}^{(2)} \approx 3 \times 10^{-19} \text{ m}^2/\text{V}$ [sample (a)], $d_{\perp}^{(2)} \approx 6 \times 10^{-19} \text{ m}^2/\text{V}$ [sample (b)], $d_{\perp}^{(2)} \approx 5 \times 10^{-20} \text{ m}^2/\text{V}$ [sample (c)]. Those values are, everything considered, in good agreement with the values experimentally measured for silver in Ref. [18].

IV. BLOCH VECTOR ANALYSIS

We now proceed to the interpretation of the results in the framework of a Bloch vector analysis. To this end, in Fig. 2 we show the Bloch vector as defined in Eq. (1) and the linear transmittance for the three samples. Both quantities are calculated for TM polarization and an incident angle of 55° , which is approximately the angle where the SH emission shows its maximum for all the samples. The first thing we note is that, differently from nondissipative structures, the

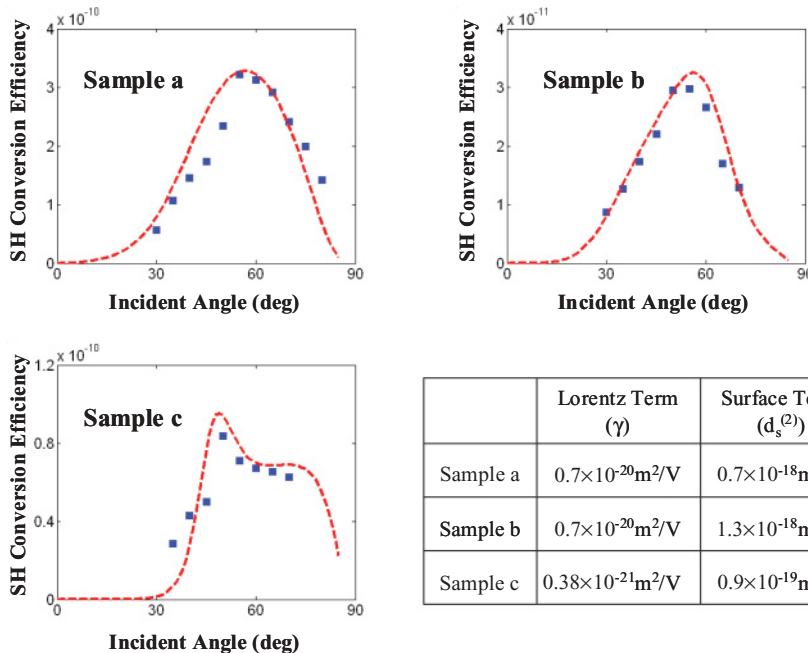


FIG. 1. (Color online) Reflected SH conversion efficiency vs incident angle for TM \rightarrow TM emission. Theory (dashed line), experiment (squares). The incident intensity is $\sim 6 \text{ GW}/\text{cm}^2$. The table shows estimated values of the quadratic nonlinearities.

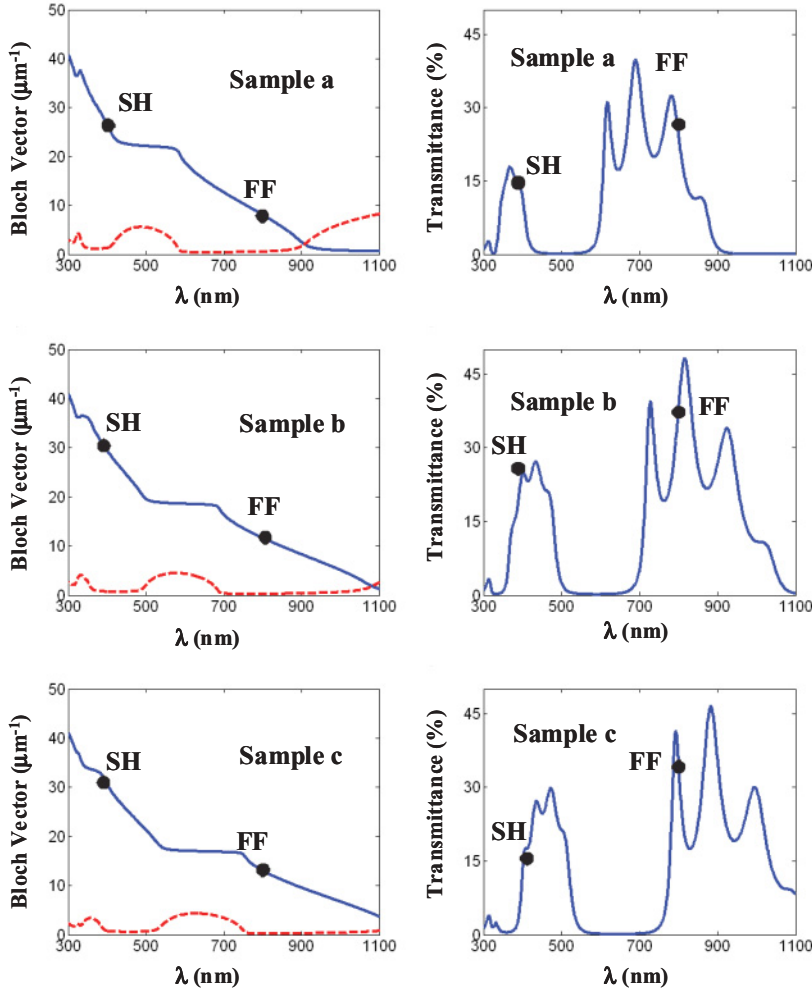


FIG. 2. (Color online) Left column, real part (continuous line) and imaginary part (dashed line) of the Bloch vector vs wavelength. Right column, linear transmittance vs wavelength for the three samples. Both quantities are calculated for TM polarization and an incident angle of 55°.

Bloch vector has an imaginary part even outside the band gaps. We also note that the real part of the Bloch vector (continuous line) closely resembles that one associated with an ideal nondissipative structure. We remark once again that, clearly, the Bloch theorem does not apply to such structures due to the dissipation and to the limited number of periods, but still a Bloch vector can be defined according to Eq. (1). Now the question is raised as to whether this generalized Bloch vector is sturdy enough to continue to give useful information on the physical phenomenon investigated even in these extreme circumstances.

In Table I we summarize the values of the real part of the Bloch vector at the FF and SH frequency and the first reciprocal lattice vector G_1 for the three samples. The phase matched case with first reciprocal lattice vector is highlighted in bold characters.

As we have already noted, if we compare sample (a) with sample (b) we find that, although they have approximately the same values of nonlinearity, sample (a)'s SH emission is one order of magnitude higher than sample (b) emission. The reason for this strong difference in the SH emission of samples (a) and (b) is clear if we resort to the Bloch vector analysis and in particular to the generalized longitudinal momentum-conservation condition (phase matching) for SH generation in periodic structures that in this case we write by resorting to the real part of the Bloch vector,

$$\pm \text{Re}K_\beta(\text{SH}) \mp 2\text{Re}K_\beta(\text{FF}) = mG_1, \tag{7}$$

where $G_1 = 2\pi/\Lambda$ is the first reciprocal lattice vector, and m is an integer that runs over all the positive and negative numbers including zero. The choice of the sign in front of the two Bloch vectors can be done independently of each

TABLE I.

	$\text{Re}K_{\beta,\text{FF}}$ (μm^{-1})	$\text{Re}K_{\beta,\text{SH}}$ (μm^{-1})	G_1 (μm^{-1})	$\text{Re}K_{\beta,\text{SH}} - 2\text{Re}K_{\beta,\text{FF}}$ (μm^{-1})	$\text{Re}K_{\beta,\text{SH}} + 2\text{Re}K_{\beta,\text{FF}}$ (μm^{-1})
Sample a	8.1	26.7	43.6	10.5	42.9
Sample b	11.7	29.5	36.7	6.1	52.9
Sample c	13.1	30.6	33.8	4.4	57.4

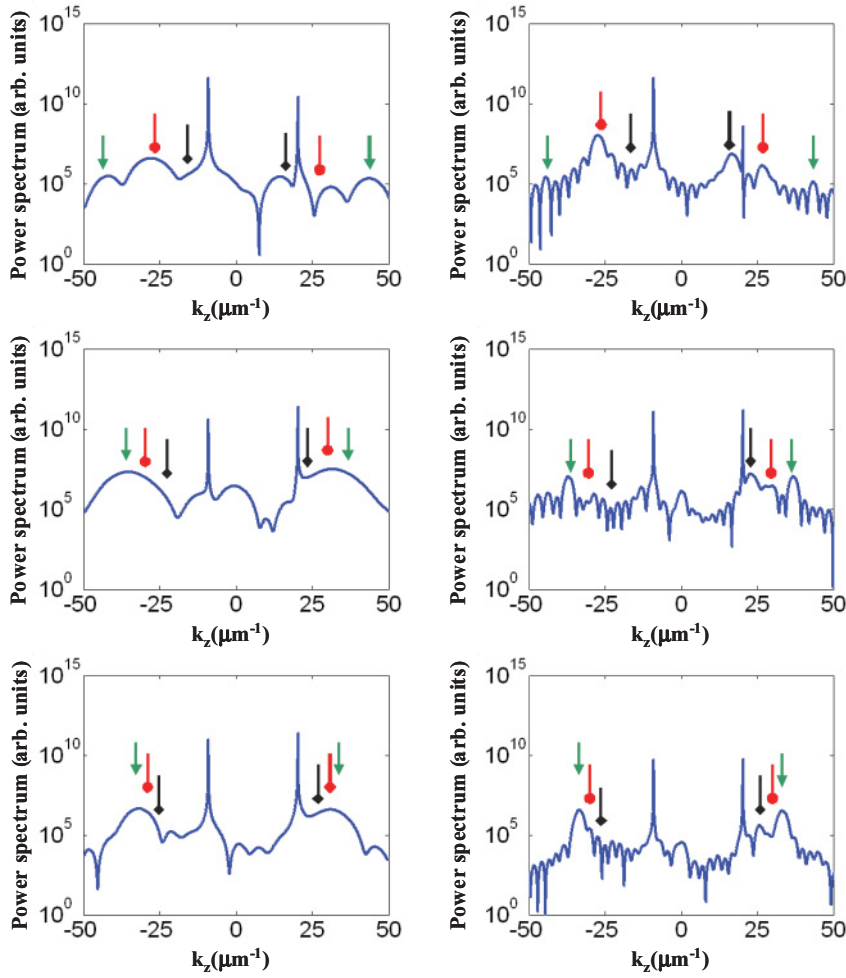


FIG. 3. (Color online) Left column, power spectrum of the SH field for the three samples. Right column, power spectrum of three hypothetical structures having the same elementary cell and same nonlinearities as the three samples, but different number of periods ($N = 15$). The positions of $\pm K_\beta(\text{SH})$ (●), $\pm 2K_\beta(\text{FF})$ (◆), and $\pm G_1$ (▼) are indicated.

other, giving, therefore, four cases: (+, −) forward SH/forward FF coupling, (−, +) backward SH /backward FF, (+, +) forward SH/backward FF, and (−, −) backward SH/ forward FF. From Eq. (7) and Table I we can realize that sample (a) is phase matched with the first reciprocal lattice vector: $\pm[\text{Re}K_\beta(\text{SH}) + 2\text{Re}K_\beta(\text{FF})] \cong \pm G_1$, while sample (b) does not satisfy any of the conditions summarized in Eq. (7). This finding by itself should confirm the applicability of the Bloch vector and clearly shows the signature of the periodicity even in finite, nonlinear, dissipative systems. However, there is more to say if we look at the power spectrum of the SH fields calculated inside the structure for the incident pump at 55° .

In Fig. 3 for $k_z > 0$ the absolute maximum for all the figures corresponds to the spectral component of the forward SH emitted in the glass substrate ($n_s \sim 1.5$): $k_z = (2\pi/\lambda_{\text{SH}})\sqrt{n_s^2 - \sin^2(55^\circ)} \cong 19.7 \mu\text{m}^{-1}$, while, obviously, for $k_z < 0$ the absolute maximum corresponds to the backward SH emitted in air, $k_z = -(2\pi/\lambda_{\text{SH}})\cos(55^\circ) \cong -13.5 \mu\text{m}^{-1}$. Apart from these two obvious components that give us information about the wave vector of the SH field *outside* the sample, the other peaks are the most important because they tell us the spectral components of the field *inside* the sample. In Fig. 3 (left column) we note that sample (a) in the backward direction has two spectral peaks of emission centered, respectively, at $-K_\beta(\text{SH})$ and $-G_1$ with the emission at $-K_\beta(\text{SH})$ predominant. In the forward direction the peaks

of emission are at $2K_\beta(\text{FF})$ and G_1 with the peak of emission at $2K_\beta(\text{FF})$ predominant. This peak at $2K_\beta(\text{FF})$ is the signature of the bound (also called inhomogeneous) SH, which, as is well known [22,23], represents the particular solution of the inhomogeneous wave equation and is generated at twice the wave vector of the pump beam, in contrast with the standard “free SH” that is generated at the wave vector of the SH. It is interesting to note that in this case the bound SH is generated at twice the pump Bloch vector; this is strong evidence of the applicability of the Bloch vector even for the inhomogeneous SH. In samples (b) and (c), all the emissions fall under the same peak and so at this stage it is not possible to discriminate which one, if any, is favored. In order to assess which of the three possible emission directions the periodicity is actually favoring, for samples (b) and (c) in particular, we have calculated the SH generated by three hypothetical structures [structures (a), (b), and (c), as shown in the right column in Fig. 3] with the same elementary cell and the same nonlinearities as our three samples, but with $N = 15$ periods. As we may expect, structure (a) follows the same path traced by sample (a); that is, the forward SH is peaked at $2K_\beta(\text{FF})$ and the backward SH is peaked at $-K_\beta(\text{SH})$. Structures (b) and (c) in this case do discriminate between the possible emissions. For sample (b) in the backward direction, the most favored emission is at $-G_1$, while in the forward direction the emission at $2K_\beta(\text{FF})$ (bound SH) and at G_1 are approximately

equally favored. Finally, for sample (c) the forward/backward emissions at $\pm G_1$ are predominant.

V. CONCLUSIONS

In conclusion, we have given experimental evidence that the Bloch vector, as defined in Eq. (1), continues to play a key role even in nonlinear phenomena involving finite, dissipative systems, such as SH generation in MD structures. Although we have reduced our study to simple 1D structures, we believe that similar considerations could be applied to multidimensional systems. In this regard, in a slightly different

context with respect to the present work, the theoretical analysis carried out in Ref. [24] where 2D dissipative gap solitons are studied is noteworthy. Nowadays, when metal-based periodic nanostructures are of central importance in the field of nanophotonics [25], our results clearly suggest that the Bloch vector still remains fundamental.

ACKNOWLEDGMENTS

We thank M. Scalora, A. Heimbeck, and M. Cappeddu for helpful discussions. G.D. and N.M. thank the National Research Council for financial support.

-
- [1] N. W. Ashcroft and N D. Mermin, *Solid State Physics* (Holt, Rinehart & Winston, New York, 1976); C. Kittel, *Introduction to Solid State Physics* (Wiley, New York, 1996).
- [2] A. Yariv and P. Yeh, *Optical Waves in Crystals* (Wiley, New York, 1984); D. L. Mills, *Nonlinear Optics* (Springer, Berlin, 1998); J. D. Joannopoulos, R. D. Meade, and J. N. Winn, *Photonic Crystals* (Princeton University Press, Princeton, NJ, 1995).
- [3] H. A. Macleod, *Thin Film Optical Filters* (Institute of Physics Publishing, Bristol, UK, 2001).
- [4] P. Yeh, *Optical Waves in Layered Media* (Wiley, New York, 1988).
- [5] V. Kuzmiak and A. A. Maradudin, Phys. Rev. B **55**, 7427 (1997), and references therein.
- [6] M. Bergmair, M. Huber, and K. Hingerl, Appl. Phys. Lett. **89**, 081907 (2006).
- [7] H. van der Lem, A. Tip, and A. Moroz, J. Opt. Soc. Am. B **20**, 1334 (2003).
- [8] D. Soto-Puebla, M. Xiao, and F. Ramos-Mendieta, Phys. Lett. A **326**, 273 (2004).
- [9] J. Zhang *et al.*, Opt. Express **15**, 7720 (2007).
- [10] E. Istrate, A. A. Green, and E. H. Sargent, Phys. Rev. B **71**, 195122 (2005).
- [11] V. S. C. Manga Rao and S. Hughes, Opt. Lett. **33**, 1587 (2008).
- [12] M. Liscidini and J. E. Sipe, J. Opt. Soc. Am. B **26**, 279 (2009).
- [13] E. D. Palik, *Handbook of Optical Constants of Solids* (Academic Press Inc., New York, 1991).
- [14] M. C. Larciprete, A. Belardini, M. G. Cappeddu, D. deCeglia, M. Centini, E. Fazio, C. Sibilia, M. J. Bloemer, and M. Scalora, Phys. Rev. A **77**, 013809 (2008).
- [15] A. A. Barybin, A. V. Mezenov, and V. I. Shapalov, J. Opt. Technol. **73**, 548 (2006).
- [16] N. Bloembergen, R. K. Chang, S. S. Jha, and C. H. Lee, Phys. Rev. **174**, 813 (1968).
- [17] Y. R. Shen, *The Principles of Nonlinear Optics* (Wiley, New York, 1984).
- [18] D. Krause, C. W. Teplin, and C. T. Rogers, J. Appl. Phys. **96**, 3626 (2004).
- [19] N. Mattiucci, G. D'Aguanno, M. J. Bloemer, and M. Scalora, Phys. Rev. E **72**, 066612 (2005).
- [20] G. D'Aguanno, N. Mattiucci, M. Scalora, M. J. Bloemer, and A. M. Zheltikov, Phys. Rev. E **70**, 016612 (2004).
- [21] J. L. Coutaz *et al.*, J. Appl. Phys. **62**, 1529 (1986).
- [22] J. Jerphagnon and S. K. Kurtz, J. Appl. Phys. **41**, 1667 (1970).
- [23] N. Bloembergen, H. J. Simon, and C. H. Lee, Phys. Rev. **181**, 1261 (1969).
- [24] H. Sakaguchi and B. A. Malomed, Phys. Rev. E **80** 026606 (2009), and references therein.
- [25] Paras N. Prasad, *Nanophotonics* (Wiley, New York, 2004).